Article

Proteomic profiling of gliomas unveils immune and metabolism-driven subtypes with implications for anti-nucleotide metabolism therapy

A list of authors and their affiliations appears at the end of the paper

Gliomas exhibit high heterogeneity and poor prognosis. Despite substantial progress has been made at the genomic and transcriptomic levels, comprehensive proteomic characterization and its implications remain largely unexplored. In this study, we perform proteomic profiling of gliomas using 343 formalin-fixed and paraffin-embedded tumor samples and 53 normal-appearing brain samples from 188 patients, integrating these data with genomic panel information and clinical outcomes. The proteomic analysis uncovers two distinct subgroups: Subgroup 1, the metabolic neural subgroup, enriched in metabolic enzymes and neurotransmitter receptor proteins, and Subgroup 2, the immune subgroup, marked by upregulation of immune and inflammatory proteins. These proteomic subgroups show significant differences in prognosis, tumorigenesis, microenvironment dysregulation, and potential therapeutics, highlighting the critical roles of metabolic and immune processes in glioma biology and patient outcomes. Through a detailed investigation of metabolic pathways guided by our proteomic findings, dihydropyrimidine dehydrogenase (DPYD) and thymidine phosphorylase (TYMP) emerge as potential prognostic biomarkers linked to the reprogramming of nucleotide metabolism. Functional validation in patient-derived glioma stem cells and animal models highlights nucleotide metabolism as a promising therapy target for gliomas. This integrated multi-omics analysis introduces a proteomic classification for gliomas and identifies DPYD and TYMP as key metabolic biomarkers, offering insights into glioma pathogenesis and potential treatment strategies.

Gliomas, accounting for around 81% of all primary central nervous system (CNS) malignancies, constitute the most common type of intrinsic brain tumor with high heterogeneity and poor prognosis[1]. Recently, gliomas have been classified into distinct subgroups according to an integrated set of molecular and histological parameters, which was initially introduced in 2016 and subsequently updated in 2021 (WHO CNS5)[2,3].

High-throughput research has been conducted with the aim of uncovering major oncogenic molecular events, identifying therapeutically actionable alterations, and delineating prognostic and

predictive subgroups among glioma patients[4–6]. Notably, these efforts have predominantly concentrated on the genomic, transcriptomic, and epigenetic dimensions[7]. At the genomic level, isocitrate dehydrogenase (IDH) mutation is a widely recognized biomarker[8]. The GLASS consortium has described other genetic alterations during glioma recurrence, such as CDKN2A deletion and hypermutations[9]. At the transcriptomic level, the Cancer Genome Atlas Program (TCGA) classified glioblastoma (GBM) into classical, mesenchymal, proneural, and neural subtypes[10]. The GLIOTRAIN discovery cohort also identified three unique patient transcriptome clusters, characterized by tumor microenvironment compositions. Although continuous efforts have been made in multi-omics research, clinical applications remain confined to a few biomarkers, such as IDH mutation, MGMT promoter methylation, and 1p/19q co-deletion[11–13]. Consequently, the development of targeted therapies and refinement of glioma classification for patient stratification remain ambitious, and are long-term goals necessitating significant progress.

Despite the substantial insights gained from DNA- and RNA-based classifications, it is anticipated that proteomic patterns, as discerned through mass spectrometry (MS), will serve as the primary conduits for elucidating biological functions in glioma[7,14,15]. In the meantime, emerging studies have demonstrated the limited correlation between protein abundance and DNA or RNA level ($r = 0.23$–0.45) in breast, colorectal, and ovarian cancer[16–18]. Intriguingly, proteins have shown superior prognostic predictive capabilities compared to their upstream mRNA counterparts[18]. Hence, the proteome, which reflects the functional consequences of genomic modifications, holds the potential to offer insights into the real state of tumor cells. In intrahepatic cholangiocarcinoma, researchers have successfully identified four subgroups characterized by unique genetic alterations, microenvironment dysregulation, tumor microbiota composition, and potential therapeutics features, with the identification of SLC16A3 and HKDC1 as prognostic biomarkers and therapeutic targets[19]. The proteomic classification of GBM has demonstrated the capacity to better reflect immune and metabolic biological processes associated with survival as compared with transcriptomic profiling[14]. Oh et al. similarly identified two proteomic clusters based on distinct Warburg-like and oxidative phosphorylation-related protein profiles, paving the way for the identification of the mTORC1/2 dual inhibitor AZD2014 as a treatment modality for GBM[7]. Collectively, these results demonstrate the value of proteomes of glioma. However, comprehensive proteomic subtyping across all four WHO-graded gliomas is still lacking, which may enhance the predictive power of clinical outcomes.

The critical role of nucleotide metabolism in driving cancer progression across various malignancies, characterized by rapid cell proliferation and genomic instability, has gained increasing recognition[20–22]. Chemotherapeutic agents such as 5-fluorouracil (5-FU) target nucleotide metabolism, underlining its significance in cancer treatment[23,24]. Recent studies have highlighted how dysregulated nucleotide metabolism affects the tumor microenvironment and immune response, offering potential for enhancing immunotherapy[25,26] Nucleotides and their metabolites can activate the immune system through host receptors, including Toll-like receptors, NOD-like receptors, adenosine receptors, and purinergic receptors[27–29]. Thus, understanding the interplay between nucleotide metabolism and the immune response is crucial for optimizing cancer therapies. In glioma research, further investigation is required to understand the diverse biological roles of hyperactive nucleotide metabolism, with the aim of developing effective combination therapies[20,30].

In this work, we present a comprehensive analysis of data from 188 glioma patients, integrating MS-based proteomic data, genomic panel data, and clinical information. We identify two distinct proteomic subgroups, the immune subgroup (S-Im) and the metabolic-neural subgroup (S-Mn), each exhibiting unique immune and metabolic-neural characteristics that correlate with patient survival.

Additionally, we discover two metabolic biomarkers, dihydropyrimidine dehydrogenase (DPYD) and thymidine phosphorylase (TYMP), which have significant prognostic and therapeutic implications, highlighting the relevance of nucleotide metabolism in glioma. Our results demonstrate the potential of proteomic classification and targeted metabolic reprogramming as promising strategies for glioma treatment.
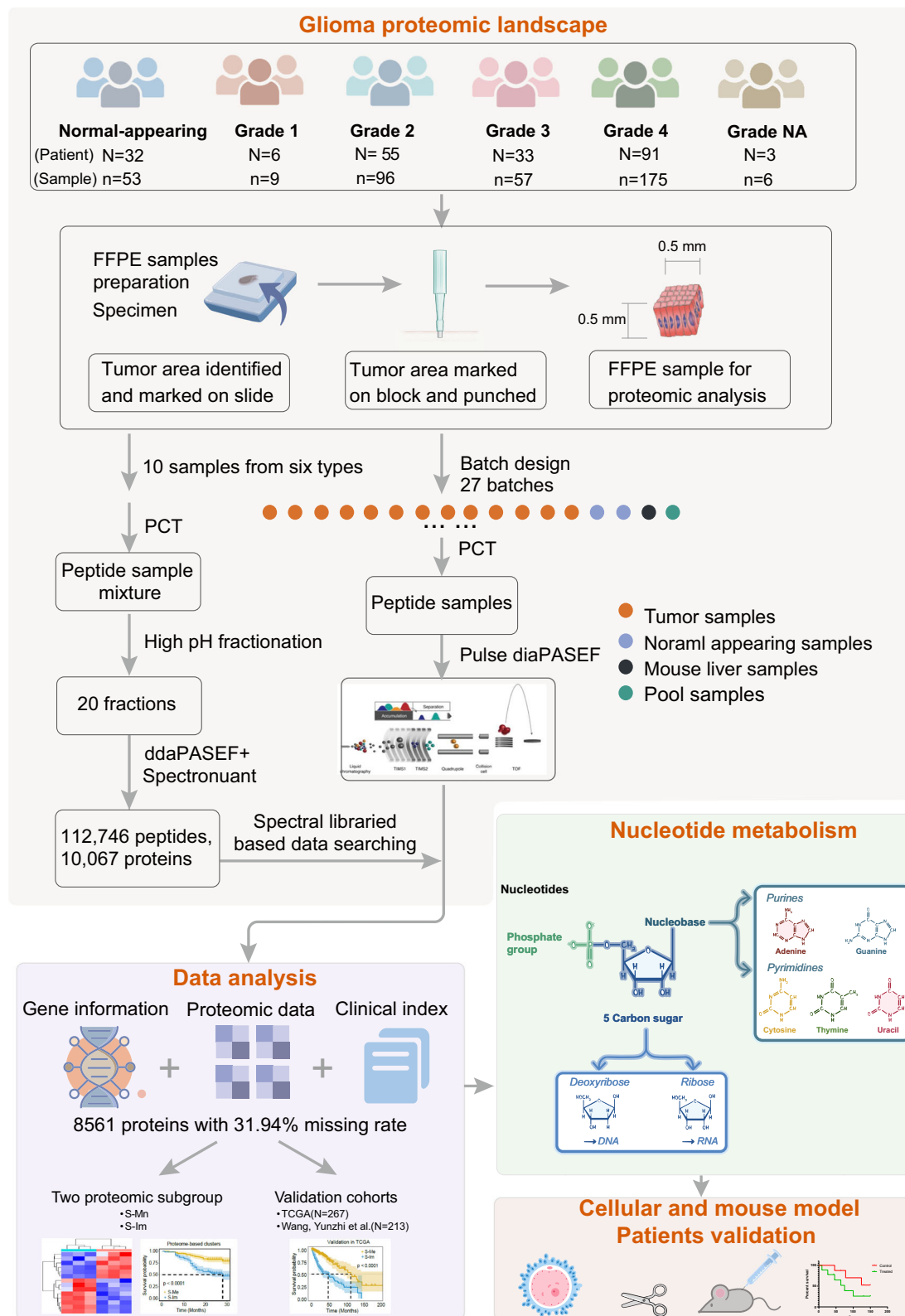
Results

Overview of glioma proteomics analyses

Proteomic profiling was performed using 343 tumor samples (including 154 biological replicates) and 53 normal-appearing brain samples from a cohort of 188 glioma patients, including 6 pilocytic astrocytoma, 51 diffuse astrocytomas (27 WHO grade 2, 14 grade 3, 9 grade 4, 1 grade NA), 47 diffuse oligodendrogliomas (28 WHO grade 2, 19 grade 3), 82 glioblastomas (WHO grade 4), and 2 not elsewhere classified[3]. Our analysis employed a well-established MS workflow, as depicted in Fig. 1. To ensure the purity of samples (tumor or normal-appearing tissue) for proteome analysis, two neuroscientists independently confirmed the punch sites, and specimens of size 0.5×0.5 mm were extracted for proteomic analysis, as shown in Supplementary Fig. S1. Clinical information, including gender, age, tumor location, WHO 2021 histology, grade, and survival, is summarized in Supplementary Data 1. The median age of the patients from whom the tumors were excised was 49.03 ± 14.48 years (range: 13–84 years), with a male-to-female ratio of 1.76:1 (male: $N = 120$; female: $N = 68$). Predominantly, the tumors were located in the frontal (99 cases) and temporal (46 cases) lobes. We obtained molecular pathology reports for 129 samples from the Department of Pathology at Huashan Hospital. These reports detail the status of IDH mutation, O6-alkylguanine DNA alkyl transferase (MGMT) promoter methylation, 1p/19q co-deletion, and telomerase reverse transcriptase promoter mutation. The remaining 59 samples were tested by immunohistochemistry only, and some marker statuses were unavailable. As of the last follow-up in September 2019, 58 patients (30.8%) had passed away, 127 (76.6%) were still alive, and 3 (1.6%) did not attend the follow-up. The median follow-up for patients alive at the last follow-up was 26.7 months.

The proteomic analysis of all glioma samples and normal-appearing brain tissues was conducted by randomly assigning them to 27 batches (Supplementary Data 2). As part of quality control measures for sample preparation and MS, we conducted correlation analyses involving mouse liver samples (Supplementary Fig. S2A) and pooled samples (Supplementary Fig. S2B), which demonstrated a strong and satisfactory correlation, affirming the reliability and robustness of our experimental procedures. The stability of the MS analysis was confirmed by the Pearson correlation between replicates' protein abundances, which was over 0.9 (Supplementary Fig. S2C). The t-SNE plots indicated the absence of any batch effect among three MS machines (Supplementary Fig. S2D), and the variance among the 27 batches was also represented in Supplementary Fig. S2E. After removing isoforms, 8561 proteins were quantified for further analyses in combination with clinical information.

Proteomic features vary among glioma clinical classifications

Next, we conducted an analysis to identify proteins with significantly different expression levels between glioma and normal-appearing brain samples. Our investigation demonstrated 570 proteins with significant differential abundance (Student's t-test, Benjamini−Hochberg (B−H) adjusted P value < 0.001, fold change > 2) (Fig. 2A). Utilizing Ingenuity Pathway Analysis (IPA), we uncovered enrichment in proteins associated with neurotransmission, synaptogenesis, neuroinflammation, tumor necrosis, and the PD-1 signaling pathway within the glioma samples, indicating the vital role of neuronal and immune-associated proteins (Fig. 2B). Recent research has reported that neuron

Fig. 1 | **Overview of glioma proteomics analyses.** A comprehensive proteomic analysis is performed on a cohort of 188 glioma patients, classified by WHO grades, including 343 tumor samples and 53 normal-appearing brain samples. Tissue specimens (0.5 × 0.5 mm) are extracted from formalin-fixed paraffin-embedded (FFPE) samples for proteomic analysis. Mouse liver samples are used as quality controls, alongside pooled samples for LC−MS/MS analysis. The analysis is conducted in 27 randomly assigned batches. The study integrates glioma genetic data, proteomic profiles, and clinical information, quantifying 8561 proteins for downstream analyses. Proteomic profiling reveals two distinct subgroups: S-Mn (metabolic-neural) and S-Im (immune), which show significant differences in prognosis within both the glioma cohort and an independent validation cohort. Metabolic pathways are explored, leading to the identification of potential biomarkers, which are validated using cellular and mouse models to confirm their accuracy and relevance. Cartoons are created with BioRender.com.
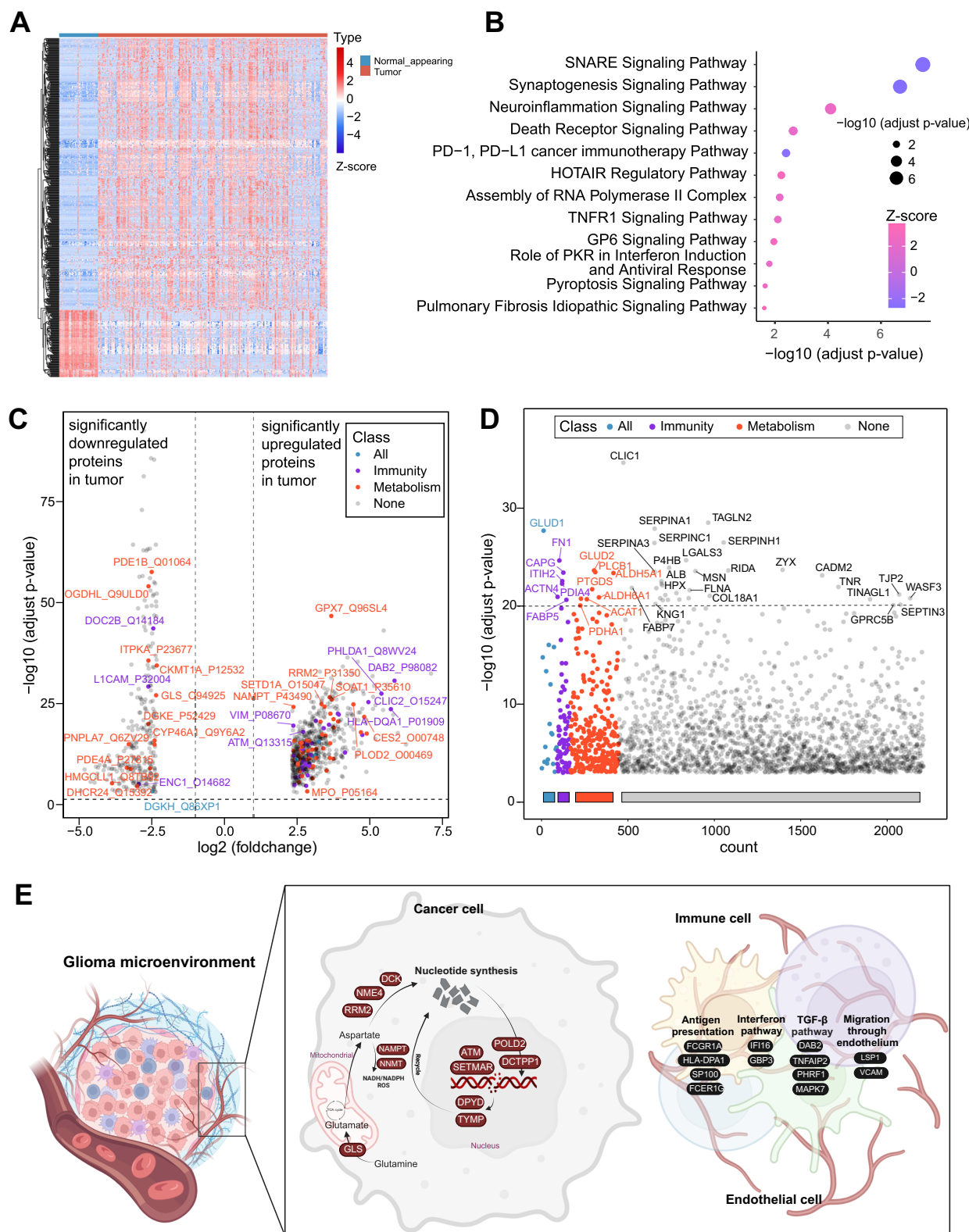
interaction with glioma cells can directly stimulate the progression and recurrence, with activation of WNT/PCP pathway and BRAF kinase[31]. Recognizing the significance of altered cellular metabolism as a communication interface between glioma cells and immune cells within the microenvironment[18,19], our subsequent focus centered on proteins related to immune regulation and metabolic processes. Among these 570 differentially expressed proteins between glioma and normal-appearing brain tissues (Student's t-test, B–H adjusted P value < 0.001, fold change > 2), we identified 28 immune-related and 51 metabolism-related proteins (Fig. 2C). Notably, the metabolism-related protein GPX7 and SOAT1, which are significantly upregulated in tumors, have been reported to lead to poor prognosis of glioma and participate in the immune regulatory process. For example, SOAT1 expression has a trend of positive correlation with Treg infiltration[32], and GPX7 may be

Fig. 2 | Proteomic features vary among glioma clinical classifications.
A Heatmap illustrates 570 differentially expressed proteins between 343 tumor samples and 53 normal-appearing brain samples (Two-sided unpaired Welch's t-test, B–H adjusted $p < 0.001$, fold change > 2). **B** Pathways are significantly enriched by IPA using the 570 differentially expressed proteins between tumor and normal-appearing brain samples (right-tailed Fisher's Exact Test, $p < 0.01$). **C** Volcano plot shows 570 differentially expressed proteins between 343 tumor and 53 normal-appearing brain samples (Two-sided unpaired Welch's t-test, B–H adjusted $p < 0.001$, fold change > 2). Immune-related and metabolism-related proteins are highlighted in red and purple, respectively (28 immune-related, 51 metabolism-related). **D** Manhattan plot displays 1047 differentially expressed proteins across four grades (one-way ANOVA test, B–H adjusted $p < 0.001$). Proteins associated with immunity and metabolism are marked in red and purple, respectively. **E** Enriched immune and metabolic processes, including nucleotide synthesis, antigen presentation, interferon signaling, and TGF-β pathways, are presented. Cartoons are created with BioRender.com. Statistical details for the relevant proteins are provided in Supplementary Data 3 (Welch's t-test, B–H adjusted $p < 0.001$, fold change > 2). Source data are provided as a Source Data file.

involved in immune mechanisms of innate immunity and adaptive immunity, type I interferon production, and regulation of synaptic transmission in low-grade glioma[33].

In addition to the obvious protein differences between normal-appearing brain and glioma tissue, we also noticed the variations in glioma protein expression across different grades and between LGG and GBM. The t-SNE plots visually depicted distinctions among these various categories (Supplementary Fig. S3A–C). Regarding histological types, the heatmap provided a clear illustration of how the differentially expressed proteins within distinct histological types of gliomas can be categorized into two distinct clusters (Supplementary Fig. S3D). Cluster 1 exhibits significant enrichment in pathways related to protein translation, such as eIF2 and eIF4, while Cluster 2 is notably enriched in pathways associated with synaptic synthesis and signal transduction pathways (Supplementary Fig. S3E, F). Additionally, there were obvious distinctions in metabolic pathways, such as amino acid, nucleotide, and lipid metabolism, between these two clusters (Supplementary Fig. S3G, H). We also observed distinct metabolic pathways, such as amino acid, nucleotide, and lipid metabolism, between these two groups (Supplementary Fig. S3G, H).

To uncover critical proteins contributing to tumor progression across various glioma grades, we identified 1047 differentially expressed proteins (ANOVA test B–H adjusted P value < 0.001) among WHO grades 1–4 glioma. Notably, these proteins associated with immune and metabolic processes displayed considerable abundance (Fig. 2D). Immune and metabolism-related proteins can be clustered into four clusters with different expression trends as the tumor grade increases (Supplementary Fig. S3I, J). They were predominantly enriched in pathways related to nucleotide synthesis, antigen presentation, interferon pathway, and TGF-β pathways, indicating intricate and complex interactions between metabolic characteristics of glioma cells and the immune microenvironment (Fig. 2E and Supplementary Data 3). Research has suggested the cross-talk between tumor metabolism and immune responses through immunometabolic rewiring[34–36], indicating that exploring the relationship between immunity and metabolism in glioma is worth studying.

Proteomic metabolic-neural and immune subtypes of glioma could predict clinical outcomes

Within our glioma cohort, we employed subtype classification based on proteome data, which is known to better reflect the disease state and underlying biology compared to genome data[14]. We firstly filtered 355 the most significantly differential expression proteins between tumor and normal-appearing brain samples (proteins with missing rates over 20% were removed, missing values were imputed by substituting them with 80% of the minimum value, B–H adjusted P value < 0.05, fold change > 3). Then through the unsupervised clustering using these proteins, the 309 tumor samples were optimally classified into two groups when the Silhouette coefficient is closer to 1 (Supplementary Fig. S4A), designated as subgroup 1 ($N = 133$) and subgroup 2 ($N = 176$). Out of 355 proteins, a total of 312 proteins showed significantly differential expression between subgroups 1 and 2 (adjusted p value < 0.05, Supplementary Data 4). Interestingly,

subgroup 1 demonstrated enrichment in both metabolic processes and neurotransmitter receptor activity, including proteins like glutaminase (GLS), glutamate receptors, GABA receptors, and calcium channels. Consequently, we have designated this group as the metabolic-neural subgroup, abbreviated as S-Mn. In contrast, subgroup 2 displayed a significant upregulation of immune and inflammatory proteins, including AKT2, CDK2, TGFB1, and IRF3, which has been named as the immune subgroup, designated as S-Im (Fig. 3A). These subtypes exhibited distinct molecular and clinical features. The proteins enriched in the S-Mn subgroup were primarily associated with synaptogenesis signaling pathway and signal transduction, among other pathways. While the S-Im subgroup exhibited an enrichment of proteins mainly involved in the PD-1 cancer immunotherapy pathway and death receptor pathways. In particular, patients in S-Mn demonstrated better clinical outcomes than those in S-Im (Fig. 3B). The principal component analysis of the diffused glioma proteome effectively stratified the two subtypes, with the first principal component distinguishing them (Fig. 3C). Single-factor logistic analysis indicated there were differences in IDH status, WHO grade, Ki-67 index between the two-subgroup proteomic groups (Supplementary Data 5), and further multivariate logistic analysis revealed that IDH status and WHO grade has little impact on two-subgroup proteomic classification (Supplementary Fig. S5).

To validate the accuracy of our proteomic classification, we utilized TCGA gene expression data ($N = 575$). Our analysis revealed that the subtypes could effectively differentiate between glioma patients (Fig. 3D), with patients from the S-Mn subtype showing a favorable prognosis, while those from the S-Im subtype displayed a poorer prognosis (Fig. 3E). Furthermore, we corroborated our proteomic classification using proteomics data from 187 glioma patients, published by Qie et al. in *Nature Communications* in 2022[37]. The heatmap displayed the top 2000 differentially expressed proteins (Fig. 3F), and Kaplan–Meier curves revealed significant prognostic differences between the S-Mn ($N = 36$) and S-Im ($N = 151$) subtypes, thereby further validating our findings (Fig. 3G). Considering the different prognoses of patients with different WHO grades (Supplementary Fig. S6A) and IDH status, we also stratified the data and performed subgroup clustering of grade 1–3 (Supplementary Figs. S4B and S6B), grade 4 (Supplementary Figs. S4C and S6C), and IDH wild-type (Supplementary Figs. S4D and S6D) patients. All the optimal grouping of patients was achieved by dividing them into two categories, with those in S-Mn demonstrating better clinical survival regardless of their WHO grade and IDH status, indicating the stability and predictive power of our proteomics subtype clustering, suggesting that two-subgroups classification is applicable to all diffuse gliomas.

Numerous studies have revealed the importance of the IDH status on the metabolic and epigenetic reprogramming of gliomas[38,39]. The significance of IDH status was officially recognized in the WHO classification of CNS tumors in 2016, where it was established as a biomarker with prognostic outcomes. In our investigation, we conducted a comparative analysis between IDH mutant ($N = 87$) and IDH wild-type ($N = 81$) gliomas across varying WHO grades, resulting in the identification of 203 differentially expressed proteins (Supplementary

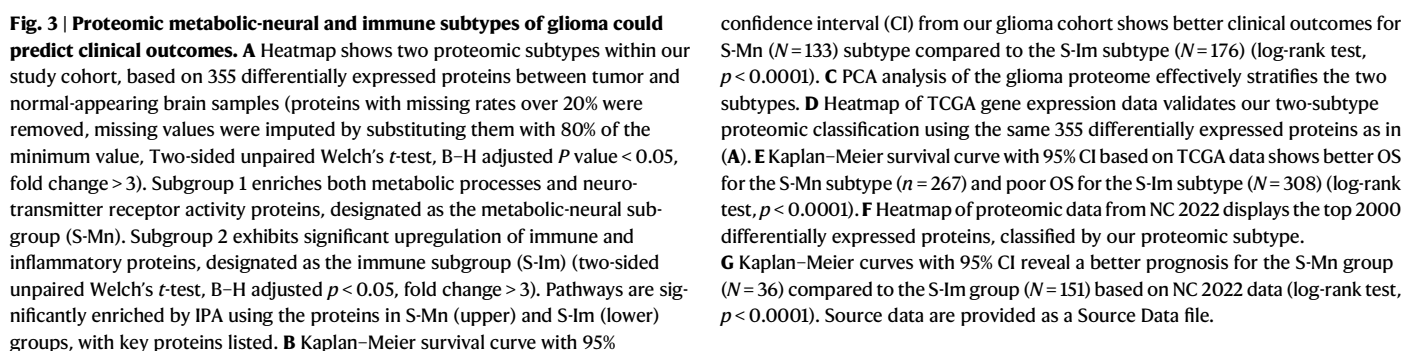**Fig. 3 | Proteomic metabolic-neural and immune subtypes of glioma could predict clinical outcomes. A** Heatmap shows two proteomic subtypes within our study cohort, based on 355 differentially expressed proteins between tumor and normal-appearing brain samples (proteins with missing rates over 20% were removed, missing values were imputed by substituting them with 80% of the minimum value, Two-sided unpaired Welch's t-test, B–H adjusted P value < 0.05, fold change > 3). Subgroup 1 enriches both metabolic processes and neurotransmitter receptor activity proteins, designated as the metabolic-neural subgroup (S-Mn). Subgroup 2 exhibits significant upregulation of immune and inflammatory proteins, designated as the immune subgroup (S-Im) (two-sided unpaired Welch's t-test, B–H adjusted p < 0.05, fold change > 3). Pathways are significantly enriched by IPA using the proteins in S-Mn (upper) and S-Im (lower) groups, with key proteins listed. **B** Kaplan–Meier survival curve with 95%

confidence interval (CI) from our glioma cohort shows better clinical outcomes for S-Mn (N = 133) subtype compared to the S-Im subtype (N = 176) (log-rank test, p < 0.0001). **C** PCA analysis of the glioma proteome effectively stratifies the two subtypes. **D** Heatmap of TCGA gene expression data validates our two-subtype proteomic classification using the same 355 differentially expressed proteins as in (**A**). **E** Kaplan–Meier survival curve with 95% CI based on TCGA data shows better OS for the S-Mn subtype (n = 267) and poor OS for the S-Im subtype (N = 308) (log-rank test, p < 0.0001). **F** Heatmap of proteomic data from NC 2022 displays the top 2000 differentially expressed proteins, classified by our proteomic subtype. **G** Kaplan–Meier curves with 95% CI reveal a better prognosis for the S-Mn group (N = 36) compared to the S-Im group (N = 151) based on NC 2022 data (log-rank test, p < 0.0001). Source data are provided as a Source Data file.

Fig. S7A). The volcano plot distinctly illustrated differential protein expression profiles between IDH mutant and wild-type gliomas (Supplementary Fig. S7B). Among them, the mitochondrial enzymes glutamate dehydrogenase GLUD1 and GLUD 2 are significantly upregulated in IDH mutant tumors, and literature also shows that high glutamate neurotransmitter flux renders cells resistant to growth-inhibitory effects of IDH mutation by supplying α-KG to fuel the citric acid cycle and support lipid synthesis[40]. In addition, glioma progression markers, such as LGALS3, FABP5, MSN, and TAGLN2 were significantly down-regulated in the IDHmut group[41–44]. Notably, our analysis revealed that metabolic processes and cytokine signaling pathways, such as lipid metabolism, fatty acid transport, DNA biosynthetic process, IL-12 signaling pathway, and IL-6 signaling pathway, were among the significantly affected pathways (Supplementary Fig. S7C). Next, we investigated the differential proteins within IDH mutant tumors at different stages. Previous studies have illuminated the substantial prognostic disparities between grade 4 and grade 2/3 astrocytomas[45,46]. Our findings indicated a significant decrease in CDK2 and IRF3 expression in grade 2/3 astrocytoma compared to grade 4, which is consistent with the established consensus that the loss of CDKN2A/B, accompanied by increased CDK activity, is intimately associated with the malignant progression of gliomas (Supplementary Fig. S7D). Finally, the cell cycle control of chromosomal replication pathway was identified as the primary differential pathway indicating the different proliferation characteristics between grade 2/3 and grade 4 astrocytomas (Supplementary Fig. S7E).

Pyrimidine metabolism is associated with glioma patients' survival

Metabolic reprogramming stands as a hallmark of cancer and represents an early event in the gliomagenesis[47,48]. For instance, GBM cells adapt to their distinctive microenvironment by upregulating enzymes associated with pyrimidine metabolism, facilitating rapid cell proliferation and DNA damage repair[49,50]. To narrow down the proteins that were more associated with survival, we selected 89 patients with long-survival (≥30 months, N = 48) and short-survival (≤12 months, N = 41). The overall survival distribution of different grade and IDH wild-type glioma was depicted in Supplementary Fig. S8A. As illustrated in the flow chart in Supplementary Fig. S8B, our initial screening process focused on identifying the differential expression proteins between tumor and normal-appearing brain samples associated with tumor metabolism in Fig. 3A. Subsequently, we conducted further screening to identify metabolic proteins that also showed a significant association with prognosis (log-rank p value < 0.05) in this cohort of 89 patients (14 metabolic proteins and 11 metabolic pathways). Meanwhile, we selected the differentially expressed proteins among four groups and were also associated with metabolism (47 metabolic proteins and 34 metabolic pathways). The intersection of these two screening stages resulted in the identification of 11 pathways, including 25 proteins. Following screened by log-rank p value < 0.05, 18 proteins were found to be both metabolically relevant and prognostically significant (Fig. 4A). All the expression levels of these 18 proteins were found to be closely associated with patients' prognosis (Supplementary Fig. S8C). We proceeded to establish a risk-scoring model based on the expression of these proteins, and Kaplan–Meier curves affirming that patients in the low-risk score group exhibited more favorable clinical outcomes (Fig. 4B). Upon further analysis of these metabolic pathways, we discovered their predominant involvement in pyrimidine metabolism, a process closely related to DNA and RNA synthesis (Fig. 4C). To validate the robustness of this model, we utilized TCGA data, yielding consistently the same prognosis conclusion as our own data (Fig. 4D). Thus, our analysis further confirmed the crucial involvement of nucleotide metabolism in controlling glioma cell behavior and patient survival and how the metabolic reprogramming especially the nucleotide metabolism contributes to tumor malignancy remained to be explored.

## DPYD and TYMP are required for GSCs proliferation and self-renewal

As illustrated in the comprehensive nucleotide metabolism map depicted in Fig. 4C highlighting proteomic-identified differential nucleotide enzymes, we found the significant roles played by catabolic enzymes within this process. The homeostasis of nucleotide metabolism requires the balance between nucleotide biosynthesis and degradation and affecting the balance of nucleotide pools could cause genomic instability and cancer progression. Among them, DPYD and TYMP are enzymes that regulate the catabolism of pyrimidine nucleosides. To explore their potential functions and mechanisms in glioma, we focused on their roles in patient-derived glioma stem cells (GSCs), which are at the top of the glioblastoma cell hierarchy and have a self-renewing effect that contributes to treatment resistance and tumor recurrence[51].

Initially, we divided patients into high- and low-expression groups based on the levels of DPYD and TYMP expression derived from our proteomic profiling. To validate the accuracy of our proteomic profiling findings, we conducted immunohistochemical (IHC) analyses on seven randomly selected patient samples from each group and the protein levels obtained from IHC were consistent with our proteomic profiling (Fig. 5A and Supplementary Fig. S9A). Subsequently, we employed two independent shRNAs to efficiently knock down the DPYD and TYMP mRNA levels in T4121 and Mes28 cells, as confirmed by real-time PCR (Fig. 5B and Supplementary Fig. S9B).

Knocking down DPYD and TYMP in GSCs markedly impaired their proliferation ability, as evidenced by reduced cell numbers on the 3rd and 5th days following knockdown (Fig. 5C and Supplementary Fig. S9C). Moreover, the self-renewal capacity of GSCs was impaired, as assessed through in vitro limiting dilution assays (Fig. 5D and Supplementary Fig. S9D) and neurosphere formation (Fig. 5E and Supplementary Fig. S9E). Specifically, the number and size of spheres significantly decreased in DPYD and TYMP knockdown GSCs (Fig. 5G and Supplementary Fig. S9F).

Given the close connection of these two proteins to DNA metabolism, and the well-known DNA damage repair capacity of GSCs, which contributes to treatment resistance (chemo drug and radiation), we evaluated the level of phospho-γH2A.X in GSCs through western blot and immunofluorescence. The knockdown of DPYD resulted in severe DNA damage and apoptosis, as indicated by an increase in phospho-γH2A.X foci within the nucleus (Fig. 5F, I) and elevated protein levels of phospho-γH2A.X and cleaved caspase-3 (CC3) (Fig. 5I). Collectively, these findings support the critical function of DPYD and TYMP in GSC maintenance and DNA metabolism.

To address the potential benefit of therapeutic targeting of DPYD and TYMP in vivo, mice bearing intracranial patient-derived GSCs tumors were transduced with a non-targeting, control shRNA (shCont) or shRNA targeting DPYD and TYMP. In particular, we aimed to investigate their roles in tumor initiation and growth. Knockdown of DPYD and TYMP significantly prolonged the survival of mice (Fig. 5J and Supplementary Fig. S9G). Subsequently, the mice were sacrificed, and their brains were subjected to hematoxylin and eosin (H&E) staining to assess glioma presence, confirming the absence of glioma growth in GSCs lacking DPYD and TYMP (Fig. 5J and Supplementary Fig. S9G). Additionally, immunohistochemical analysis of pathological sections from 43 glioblastoma (GBM) patients revealed that high-expression levels of DPYD and TYMP were associated with poor prognosis (Fig. 5K, Supplementary Fig. S9H and Supplementary Data 6). Together, these findings have revealed the significance of DPYD and TYMP in the initiation and growth of glioma in vivo, there thereby reinforcing the importance of targeting nucleotide metabolism as a potential strategy for the treatment of glioma.
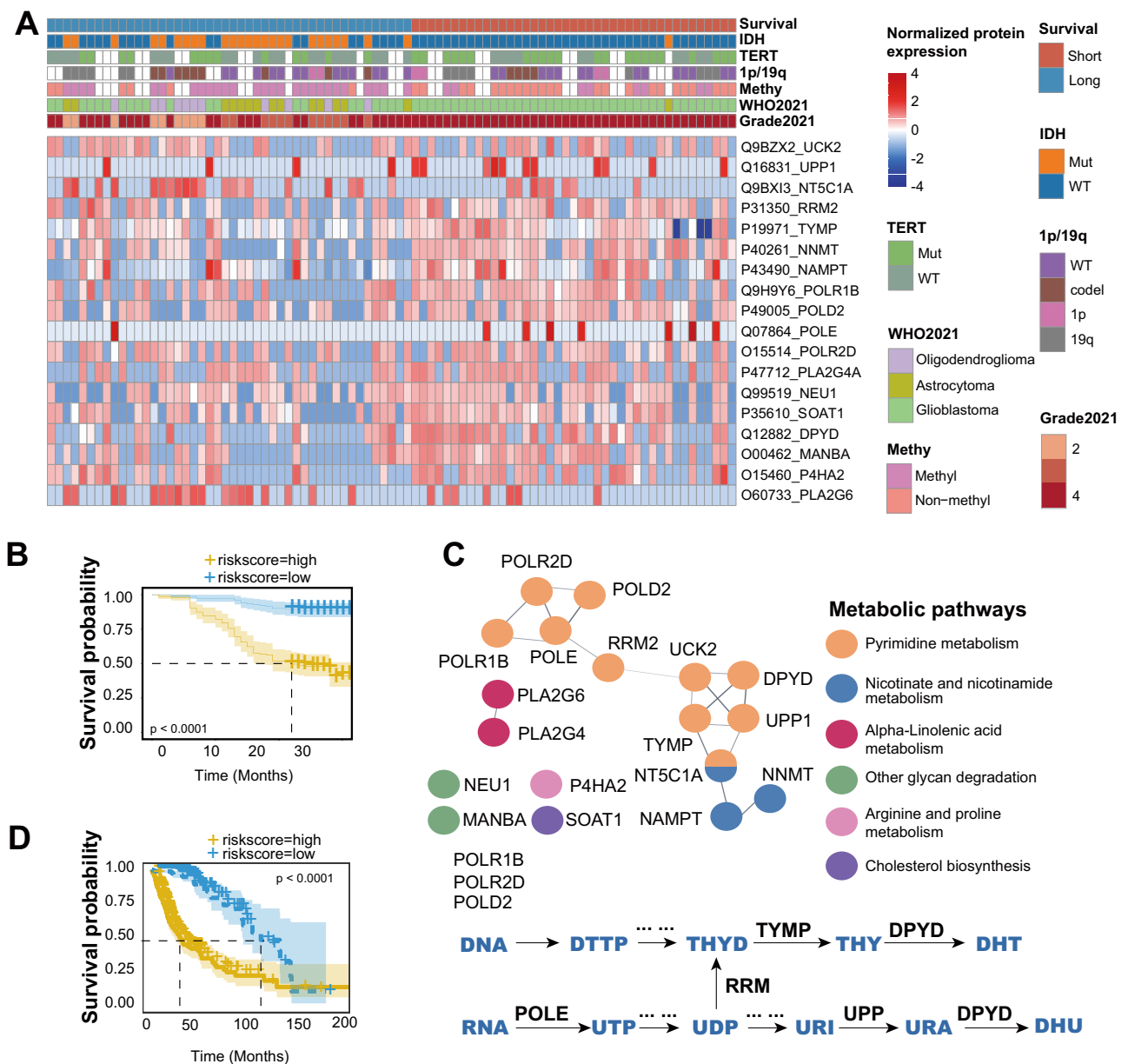
Fig. 4 | Pyrimidine metabolism associate with glioma patients' survival.
**A** Heatmap shows 18 different expressed proteins between the long-survival ($N = 48$) and short-survival ($N = 41$) groups, filtered through the methods shown in Supplementary Fig. S8B. **B** Kaplan–Meier survival curve with 95% CI (high-risk group, $N = 41$; low-risk group, $N = 48$) illustrates the risk-scoring model based on these 18 proteins (log-rank test, $p < 0.0001$). **C** Pathway enrichment analysis indicates that pyrimidine metabolism is predominantly involved. **D** Kaplan–Meier survival curve with 95% CI using TCGA data (high-risk group, $N = 288$; low-risk group $N = 287$) validates the risk-scoring model (log-rank test, $p < 0.0001$). Source data are provided as a Source Data file.

Discussion

In this study, we conducted a large-scale proteomic analysis of gliomas, with a specific focus on uncovering the immune and metabolic heterogeneity within these tumors, while also exploring proteome-based subtyping. Our investigations led to the identification of two distinct proteomic subtypes within diffuse glioma, each characterized by unique immune and metabolic features. Importantly, these subtypes demonstrated a robust association with clinical outcomes. In addition, we validated the effectiveness of our proteomic subtyping approach using data sourced from the TCGA database. Our biological experiments also revealed the critical roles of DPYD and TYMP in promoting the proliferation and self-renewal of GSCs, making them potential targets for precision treatment strategies.

For many years, adult malignant gliomas have been managed using uniform approaches, regardless of their molecular characteristics, often following the conventional Stupp regimen[50]. While significant progress has been made in understanding glioma development at the DNA and RNA levels, the establishment of targeted therapies tailored to specific molecular profile, such as IDH mutant or VEGF expression gliomas, has remained elusive. We propose that, given the primary role of proteins in executing physiological functions within organisms, a proteome-based approach may uncover signaling pathways that could pave the way for the development of innovative therapeutic strategies. Indeed, there is increasing evidence in the literature that supports the existence of distinct metabolic proteomic subtypes in glioblastoma based on aerobic/anaerobic energy metabolism[7,52].
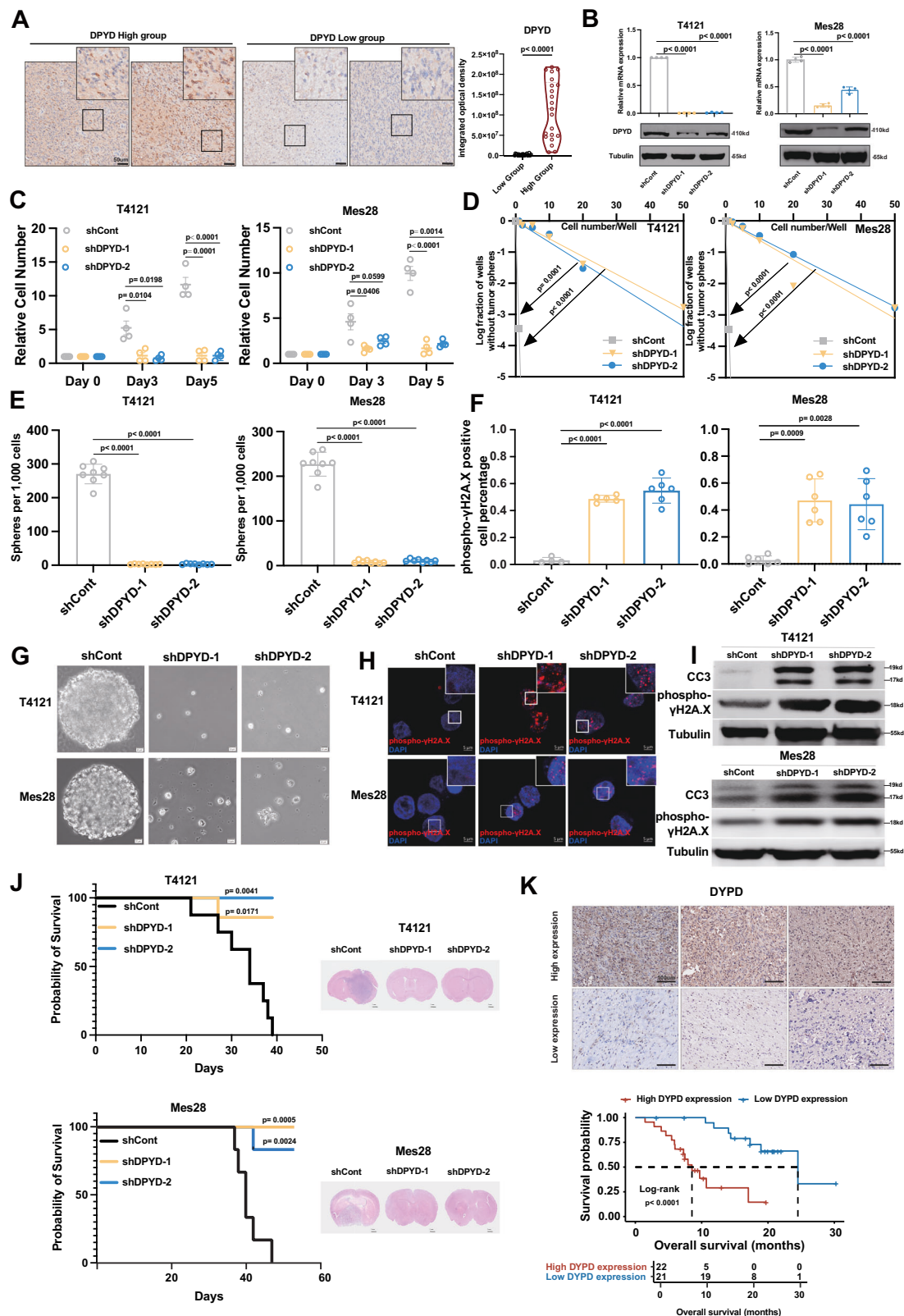
We have made several significant discoveries in our study. Firstly, we identified key proteins that distinguish between normal-appearing brain tissue and glioma tissue, with a focus on pathways related to synaptic synthesis, neuroinflammation, and PD-1 pathways. These pathways are closely associated with tumor metabolism and immune inflammation. Furthermore, we categorized WHO grade 2–4 gliomas into two subtypes based on proteomic differences, revealing significant disparities in patient survival between these subtypes. Notably, this proteomic classification remained robust across varying tumor WHO grade and IDH status. To further explore the underlying prognostic mechanisms, we selected differentially expressed proteins associated with metabolism for subsequent analysis and investigation.

Metabolic reprogramming stands as a well-established hallmark of cancer, and the growing understanding of the cross-talk between

Fig. 5 | DPYD is required for GSC proliferation and self-renewal. A IHC validation of dihydropyrimidine dehydrogenase (DPYD) expression based on proteomic profiling. The optical density of IHC staining is measured quantitatively, confirming the different expression between the two groups (high group, $N = 21$; low group, $N = 21$; Student's t-test, $p < 0.0001$; scale bar = 50 μm). **B** DPYD mRNA levels and protein levels in T4121 and Mes28 cells after knockdown show an efficiency greater than 50% (mRNA, mean ± SEM, $N = 4$; Student's t-test; in T4121, shCont vs shDPYD-1, $p < 0.0001$ and shCont vs shDPYD-2, $p < 0.0001$; in Mes28, shCont vs shDPYD-1, $p < 0.0001$ and shCont vs shDPYD-2, $p < 0.0001$). **C** Proliferation assay demonstrates that targeting DPYD impairs proliferation, as assessed by cell number on day 3 (mean ± SEM, $N = 4$, Student's t-test; in T4121, shCont vs shDPYD-1, $p = 0.0104$ and shCont vs shDPYD-2, $p = 0.0198$; in Mes28, shCont vs shDPYD-1, $p = 0.0406$ and shCont vs shDPYD-2, $p = 0.0599$). GSC proliferation is significantly inhibited on day 5 (mean ± SEM, $N = 4$, Student's t-test; in T4121, shCont vs shDPYD-1, $p = 0.0001$ and shCont vs shDPYD-2, $p < 0.0001$; in Mes28, shCont vs shDPYD-1, $p = 0.0001$ and shCont vs shDPYD-2, $p = 0.0014$). **D** In vitro limiting dilution assays (analysis was performed using software available at http://bioinf.wehi.edu.au/software/elda with simple line regression; in T4121, shCont vs shDPYD-1, $p < 0.0001$ and shCont vs shDPYD-2, $p = 0.0001$; in Mes28, shCont vs shDPYD-1, $p < 0.0001$ and shCont vs shDPYD-2, $p < 0.0001$) and (**E, G**) tumorsphere formation reveal impaired self-renewal of DPYD knockdown GSCs. Sphere number (**E**, mean ± SEM, $N = 8$, Student's t-test; in T4121, shCont vs shDPYD-1, $p < 0.0001$ and shCont vs shDPYD-2, $p < 0.0001$; in Mes28, shCont vs shDPYD-1, $p < 0.0001$ and shCont vs shDPYD-2, $p < 0.0001$) and size (**G**, scale bar = 20 μm) are significantly decreased in DPYD knockdown GSCs. **H, F** Immunofluorescence shows increased phospho-γH2A.X foci in the nucleus of GSCs after DPYD knockdown, indicating severe DNA damage (**F**, mean ± SEM, $N ≥ 4$, Student's t-test in foci > 15 as positive; in T4121, shCont vs shDPYD-1, $p < 0.0001$ and shCont vs shDPYD-2, $p < 0.0001$; in Mes28, shCont vs shDPYD-1, $p = 0.0009$ and shCont vs shDPYD-2, $p = 0.0028$). The percentage of phospho-γH2A.X positive cell percentage is calculated, indicating elevated DNA damage after DPYD knockdown. **I** Western blot shows increased protein levels of phospho-γH2A.X and Cleaved Caspase-3 (CC3) proteins following DPYD knockdown. **J** Knockdown of DPYD in T4121 (each group, $N = 8$) and Mes28 (each group, $N = 6$) significantly increases mouse survival (log-rank test; in T4121, shCont vs shDPYD-1, $p = 0.0171$ and shCont vs shDPYD-2, $p = 0.0041$; in Mes28, shCont vs shDPYD-1, $p = 0.0005$ and shCont vs shDPYD-2, $p = 0.0024$). H&E staining of mouse brain shows that DPYD inhibition suppresses GSC growth ($N = 3$, scale bar = 1 mm). **K** An external validation of another cohort of glioma patients ($N = 43$) confirms differential expression by IHC, and the Kaplan−Meier survival curve shows poor prognosis in the high DYPD expression group (log-rank test, $p < 0.0001$; scale bar = 100 μm). Source data are provided as a Source Data file.

metabolism and cancer epigenetics expands our insights into the contributions of metabolic derangements to tumor malignancy. Within this context, pyrimidine metabolism has emerged as a promising vulnerability in IDH mutant glioma. For example, BAY 2402234, an inhibitor targeting dihydroorotate dehydrogenase in pyrimidine synthesis, has exhibited the capacity to sensitize DNA damage in response to nucleotide pool imbalance, thus influencing clinical outcomes in patients[53,54]. However, the maintenance of a dynamic DNA metabolism pool requires not only enzymes involved in anabolism but also those participating in catabolism. In our investigation, we unveiled the critical role played by pyrimidine catabolism enzymes in glioma, and notably, their association with clinical prognosis, which is consistent with the current prevailing understanding in the field. Our study provides a valuable contribution to the field of cancer research by highlighting the critical importance of nucleotide metabolism in cancer cells and the potential of targeting this metabolic dependency as an effective cancer therapy strategy. DPYD, which serves as the initial committed step in pyrimidine degradation, has been extensively investigated, particularly in the context of 5-FU metabolism, a widely used chemotherapy drug. Altered DPYD activity in the context of tumorigenesis may disrupt the balance of nucleotide pools within cells, potentially leading to genomic instability and contributing to cancer development. Notably, in glioma research, studies have demonstrated elevated DPYD expression in diffuse midline gliomas compared to normal astrocytes, indicating resistance to 5-FU treatment and underscoring the malignant phenotype of glioma biology[55]. Furthermore, in pancreatic cancer, a disease exhibiting similar aggressiveness like glioma, the inhibition of STAT3-DYPD expression by chemopreventive agent has demonstrated the capacity to restrain tumor proliferation[56]. Beyond its influence on tumor cell proliferation, DPYD has been implicated in maintaining a mesenchymal-like state in epithelial tumors by directing pyrimidine metabolites towards the catabolic pathway[57]. TYMP encodes the enzyme thymidine phosphorylase, an enzyme that exhibits overexpression in various cancer types, with established roles in tumor growth, invasion, and chemotherapy resistance[58–60]. Beyond its primary role in thymidine metabolism, TYMP serve as a potent angiogenic factor and functions as a cytokine that stimulates endothelial cell proliferation and migration, thereby promoting the formation of new blood vessels[61]. This angiogenic activity of TYMP holds particularly relevant in the context of glioma, given that tumor growth and invasion critically depend on the development of a robust blood supply. Elevated TYMP levels have

been associated with increased vascularity and more aggressive tumor behavior. In general, our study provided experimental validation of the roles of DPYD and TYMP, which have traditionally been investigated primarily in the context of chemotherapy response within the malignant progression of glioma. These findings demonstrated that the downregulation of these two enzymes significantly reduces the self-renewal capacity of GSCs, ultimately leading to DNA damage, apoptosis, and impairments of in vivo tumorigenesis, which strongly suggest that DPYD and TYMP might contribute to the genesis of glioma through mechanisms distinct from their known involvement in drug metabolism. Moreover, considering the widespread use of drugs targeting these two enzymes in preclinical gastrointestinal and urinary tumor models[62–65], conducting clinical trials to evaluate the efficacy of these drugs in glioma patients represents a promising direction for future research.

Our study has some limitations that should be acknowledged. First, our analysis only measures protein expression, and does not account for post-translational modifications, such as phosphorylation and glycosylation, that may also affect glioma pathogenesis. Second, our proteomic subtyping approach needs to be validated in larger cohorts to increase its robustness. Third, more research is needed to elucidate the exact molecular pathways and downstream effectors of DPYD and TYMP in glioma development.

In conclusion, our study provides insights into the molecular mechanisms of glioma and identifies potential biomarkers and therapeutic targets. Proteomic subtyping emerges as a more accurate predictor of patient prognosis in glioma. Notably, enzymes involved in pyrimidine catabolism, specifically DPYD and TYMP, emerge as pivotal players in glioma pathogenesis. Further research is warranted to validate and expand upon these findings, with the aim of improving the diagnosis and treatment of this devastating cancer.

Methods

This study was approved by the Ethics Committee of Huashan Hospital (KY2021-064). Patients provided informed consent, agreeing to donate tumor samples and to the publication of clinical information for research purposes.

Clinical samples collection and preparation

Formalin-fixed and paraffin-embedded (FFPE) human brain glioma samples were obtained from the Department of Neurosurgery, Huashan Hospital of Fudan University during January to December 2018.

The specimens were diagnosed and graded according to WHO guidelines by two neuropathologists[3]. Patients provided informed consent (KY2015-256) before surgery, agreeing to donate tumor samples and personal information for research purposes. The acquisition and use of human glioma samples were approved by the Ethics Committee of Huashan Hospital (KY2021-064) and adhered to ethical principles outlined in the Helsinki Declaration (1964, amended in 2013) and the guidelines of the World Medical Association[66]. A total of 188 glioma patients were included in the study, with a male-to-female ratio of 1.76:1 (120 males, 68 females).

For the subsequent proteomic analysis, two neuroscientists selected representative histological area of either the tumor or normal-appearing tissue based on H&E staining slides, ensuring sample purity for punching. Areas displaying hemorrhagic, necrotic, or degenerative changes, such as mucous or cystic changes, were deliberately excluded from the punching process. Normal-appearing brain tissue samples (53 samples from 32 cases) were included as controls. All samples were obtained using a 1 mm biopsy punch (Kai medical, #BP-10F) for MS analysis. To minimize potential bias from tumor heterogeneity, portions of FFPE samples were punched at two independent sites.

Hematoxylin and eosin (H&E) staining
The FFPE tissues were sliced into 4 μm sections, and H&E staining was performed following standard protocols using the fully automated BOND-III stainer system (Leica Biosystems, USA).

Peptide sample preparation
Protein extraction and peptide digestion were performed as described previously[67,68]. Briefly, the FFPE tissue samples were dewaxed by heptane and hydrated with a gradient ethanol solution. Proteins were extracted from the tissues and then enzymatically digested into peptide samples using trypsin (Hualishi Scientific, China) and LysC (Hualishi Scientific, China) relying on PCT (Pressure Biosciences Inc., MA, USA)[67,68].

Liquid chromatography-tandem mass spectrometry (LC−MS/MS)
Clean peptide samples were separated with a nano Elute system (Bruker Daltonics, Germany) at a flow rate of 300 nL/min, at 217.5 bar. The linear liquid phase gradient of buffer B was 5–27% for 90 min during the data-dependent acquisition (DDA) mode and then for 60 min during the PulseDIA acquisition. The mobile phase was mixed with buffer A (2% ACN, 0.1% formic acid) and buffer B (98% ACN, 0.1% formic acid). Peptides were scanned by a Captive Spray nanoelectrospray ion source on a hybrid trapped ion mobility spectrometer (TIMS) quadrupole time-of-flight mass spectrometer (TIMSTOF Pro, Germany).

To generate a library of ion mobility-enhanced spectra, we performed the DDA of the Parallel Cumulative Sequential Fragmentation (PASEF) mode with 10 PASEF scans every top-N acquisition cycle. A total cycle time of 1.17 s was achieved with an accumulation and ramp time of 100 ms each for the dual TIMS analyzer. The ion mobility was scanned from 0.6 to 1.6 V/cm^2. The MS1 and MS2 acquisitions were performed in the m/z range of 100–1700 Th. Precursors reaching a target value of 20,000 arbitrary units were dynamically excluded for 0.4 min, and singly charged precursors were excluded at positions in the m/z-plane of ion mobility.

The peptide samples were analyzed using the PulseDIA mode[69] of the diaPASEF[70]. Ion mobility was scanned from 0.7 to 1.3 V/cm^2. MS1 and MS2 acquisitions were performed in the m/z range of 100–1700 Th. We defined two sets of complementary isolation windows and applied them to the two MS methods for two injections. We set a window with a width of 25, and the rest of the parameters were the same as for the DDA.

High-pH reversed-phase chromatography fractionation
Approximately 100 μg of peptide mix of glioma tumor and normal-appearing brain were fractioned on a chromatographic column (BEH C18, 300 Å, 5 μm, 4.6 mm × 250 mm) coupled to a Thermo Dionex Ultimate 3000 (Thermo Fisher Scientific, USA). A linear gradient of 5−35% buffer B (98% ACN, 0.6% ammonia, pH = 10) was kept for 68 min to generate 60 fractions. The fractions were next combined into 20 samples according to a published strategy[71]. Finally, all samples were dried by a SpeedVac (Thermo Fisher Scientific, USA), reconstituted in 0.1% formic acid, and spiked with standard peptides (iRT, Switzerland).

Human glioma-specific spectral library generation and proteomic data analysis
The 20 glioma DDA data files and 88 normal brain DDA data files were analyzed using Spectronaut (version 14.5). The background FASTA file was downloaded from SwissProt on 22 January 2020 and contained 20,365 human protein entries. The tolerance for fragment and precursor was set to dynamic, which depends on each file. The digestion enzyme was trypsin, cutting after "KR" but not before "P." False discovery rates (FDRs) of peptide-spectrum matches, precursors, and proteins were set to 1%. A total of 17,0445 precursors and 10,067 proteins were identified in this spectral library. The self-constructed library was further used for the PulseDIA data analysis by Spectronaut (version 14.5) without cross-run normalization. FDRs of precursors and proteins were set to 1%. Other settings were used as default parameters. Missing values were imputed by 0.8 times the minimum intensity found in the matrix of 8561 proteins.

Proteomic data quality control analysis
To minimize the batch effect, the 343 tumor and 53 normal-appearing brain samples were randomly separated into 27 batches each (Supplementary Data 2) for proteomic data acquisition. During sample preparation, from batches 1 to 25, each batch contained 13 tumor samples, two normal-appearing brain samples, and one mouse liver sample for PCT quality control; batch 26 included ten tumor samples, two normal-appearing brain samples, and one mouse liver sample; batch 27 included nine samples contaminated by blood and one mouse liver sample. Additionally, for the LC−MS/MS acquisition, each batch contained one pooled peptide sample and one randomly selected peptide sample as a replicate for the LC−MS/MS technical quality control.

Differentially expressed analysis
A two-sided unpaired Welch's t-test was used to compare the two groups. And p values were adjusted using the B−H method. The differentially expressed proteins between two groups were filtered with fold change and B−H adjusted p value, while among over two groups were filtered with one-way ANOVA p value. The pathway enrichment analysis was performed using differentially expressed proteins among different groups. The activation degree score of the pathway is calculated in IPA.

Proteomic-based clustering analysis
To determine the optimal number of subtypes, we utilized K-means clustering (implemented through the "kmeans" function in R) and consensus clustering (implemented through the "consensusClusterPlus" package in R). In order to cluster the samples based on the constituent pattern of each pathway, we scaled each sample. Consensus clustering was then employed to evaluate the robustness of the K-means clustering, with 1000 iterations and 80% resampling. Finally, a silhouette analysis was performed to confirm the stability of the clustering. The best method was used for clustering all samples.

Cell culture and reagents

Patient-derived GSCs (T4121 and Mes28) were derived by our laboratory and obtained via a material transfer agreement with Duke University. These GSCs were cultured in Neurobasal media (Thermo Fisher Scientific, #21103049) supplemented with 2% B27 supplement without vitamin A (Thermo Fisher Scientific, # 12587010), EGF and bFGF (20 ng/mL each; R&D Systems, #236-EG and # 3718-FB), 1% sodium pyruvate (Thermo Fisher Scientific, #11360070), and 1% GlutaMAX (Thermo Fisher Scientific, #35050079). In addition, 293T cells (sourced from ATCC) were cultured in Dulbecco's modified Eagle's medium (Thermo Fisher Scientific, #11965092) with 10% fetal bovine serum (Thermo Fisher Scientific, #A4766801).

Plasmids and lentiviral transduction

Two non-overlapping shRNAs targeting human DPYD (target sequences: GCCGTATGATGTAGTGAATTT and GCAATTTGCTACTGAGGT ATT), TYMP (target sequences: GCCTCCATTCTCAGTAAGAAA and GCTGGAGTCTATTCCTGGATT), and a non-targeting control shRNA (shCont, CCTAAGGTTAAGTCGCCCTCG) were construed into a PLKO.1 plasmid. To generate lentiviral particles, we employed 293T cells and conducted co-transfection with the packaging vectors psPAX2 (Addgene, #12259) and pMD2.G (Addgene, #12259) using the polyethylenimine transduction method in the OPTI-MEM medium (Thermo Fisher Scientific, #31985062). After 8 h, the medium was changed. The supernatants containing the viruses were collected in a 50 mL tube at 24, 48, and 72 h after transfection, filtered and concentrated by PEG8000 (Sigma, # 89510) precipitation. Cells were then infected with lentiviruses for further experiments with 8 µg/mL polybrene which enhances infection efficiency. Stable cells were selected with media containing 2 µg/mL puromycin. The stable cells were detected by qRT-PCR and immunoblotting.

Quantitative RT-PCR

An RNA purification kit (EZB, #B0004DP) was used to isolate total cellular RNA from cell pellets. The 4× EZscript Reverse Transcription Mix II with gDNA remover (EZB, RT2GQ) was utilized to reverse cDNA transcription. Quantitative real-time PCR was performed on the QuantStudio 6 Flex Real-Time PCR System (Thermo Fisher Scientific) with a 2× S6 universal SYBR qPCR mix (NovaBio, #Q204). The primer pairs for qPCR in this study were as follows: human DPYD forward 5′-GCTGTCCCTGAGGAGATGGA-3′ and reverse 5′- GTCCGAACAAA CTGCATAGCAA-3′; TYMP forward 5′-CACCTTGGATAAGCTGGAGTC-3′ and reverse 5′-GGCTGCATATAGGATTCCGTC-3′; ACTIN forward 5′-T CCCTGGAGAAGAGCTACG-3′ and reverse 5′-GTAGTTTCGTGGATGCC ACA-3′.

Western blot

Equal cell amounts per group were collected and boiled in sodium dodecyl-sulfate polyacrylamide gel electrophoresis loading buffer. Electrophoresis was performed using 12% protein gels, followed by transfer onto polyvinylidene fluoride membrane. TBST supplemented with 3% bovine serum albumin (BSA) was used for blocking for 1 h at room temperature. Blotting with primary antibody was performed at 4 °C overnight. The following antibodies were used: DPYD (1:1000, Abcam, ab134922), anti-Cleaved Caspase-3 (1:1000, CST, #9661), anti-phospho-γH2A.X (1:1000, CST, #9718), and anti-α-Tubulin (1:5000, Proteintech, #66031-1-lg). A secondary antibody (1:2000, Proteintech, #SA00001-2 and #SA00001-1) was applied to bind with the primary antibody for 2 h. Finally, membranes were visualized under an enhanced chemiluminescence detection system (Typhoon FLA 9500, GE Healthcare).

In vitro limiting dilution assay

In vitro limiting dilution was performed following established protocols[72,73]. Briefly, decreasing numbers of cells per well (50, 20, 10, 5, and 1) were plated into 96-well plates. Seven days after plating, the presence and count of neurospheres in each well were recorded. An extreme limiting dilution analysis was performed using software available at http://bioinf.wehi.edu.au/software/elda[72,73].

Cell proliferation and neurosphere formation assay

Cell proliferation experiments were conducted by seeding the cells of interest at a density of 10,000 cells/well in 12-well plates, with four replicates for each condition. Cell counts were performed on day 3 and day 5 to assess cell proliferation. The neurosphere formation was measured by seeding 5000 cells into a 12-well plate with eight replicates for each group. The presence and quantity of tumor spheres in each well were recorded 7 days after plating.

Immunohistochemistry (IHC) staining

The IHC staining procedures followed established protocols[74]. In brief, 3% H_2O_2 was used to quench endogenous peroxidases, followed by antigen retrieval using the citrate buffer. Primary antibodies against DPYD (1:500, Proteintech, #27662-1-AP) and TYMP (1:200, Proteintech, #12383-1-AP) were incubated overnight at 4 °C. Staining was carried out using an LSAB IHC kit (DAKO Cytomation, #VB-6017D), with 3,3-diaminobenzidine as the chromogen and Mayer's hematoxylin for nuclear staining.

For semi-quantitative analysis of the IHC staining, three randomly selected fields (100 µm^2 each) were chosen from each sample, and images were captured using a charge-coupled device camera. Staining intensity was analyzed using IMT i-Solution software version 10.1 (IMT i-Solution, Inc., Canada), as previously described[75]. The results of IHC image analysis were presented as mean ± SEM. Based on the IHC staining density, cases were categorized into a high-expression group with staining intensity above the average value and a low-expression group with staining intensity below the average value.

Immunofluorescence staining

For immunofluorescence microscopy, cells were digested into single cells and then collected. Cells were fixed with 4% paraformaldehyde twice for 30 min at room temperature, followed by permeabilization using 0.01% Triton X-100 (Thermo Fisher Scientific, # HFH10) for 10 min, then blocked in 3% BSA at room temperature for 30 min. Next, cells were incubated with anti-phospho-γH2A.X (1:500, CST, #9718) antibodies at 4 °C overnight. After washing with PBS, cells were stained with the second antibody conjugated with Alexa Fluor 647 (1:1000, Invitrogen, #A32733) at 37 °C for 1 h. Nuclei were stained with DAPI (1:500, Sigma, MBD0015). After adding the Fluoromount-G (SourthenBiotech, #0100), the cells were examined using a Zeiss LSM900 confocal microscope. All imaging results were processed using the ImageJ software. Phospho-γH2A.X foci were quantified in individual nuclei, with least 50 nuclei counted for foci quantification in each group.

In vivo tumorigenesis

In the knockdown experiment, GSCs were transduced with lentiviral vectors expressing shDPYD, shTYMP, and a non-targeting control shRNA (shCont). After 48 h of infection, cells were assessed by qPCR and western blot to confirm successful knockdown. Then the cells were counted and randomly implanted into the right cerebral cortex of healthy, 4–6 weeks old male mice of Balb/c nude background purchased from the GemPharmatech Company in Jiangsu Province. All mice experiments were performed following an animal protocol approved by the Institutional Animal Care and Use Committee of the Shanghai Medical College, Fudan University. All experimental mice were housed in a specific pathogen-free environment with ambient temperature of 20–26 °C and humidity of 30–70% in a 12 h light/12 h dark cycle, with no more than 5 mice per cage. The animals were sacrificed at the point that they displayed neurological symptoms, in

accordance with the protocol outlined by the NIH Office of Animal Care and Use. The brains were collected, fixed in 4% formaldehyde, paraffin-embedded, and then sectioned. These sections were stained with H&E for histological analysis. In parallel survival experiments, animals were monitored until they developed neurological signs.

Statistical analysis

All analyses were performed using R statistical software (R-4.1.1) and SPSS (version 19.0; SPSS Inc., USA). Unless otherwise specified, all tests were two-tailed, and P values less than 5% were considered statistically significant.

Reporting summary

Further information on research design is available in the Nature Portfolio Reporting Summary linked to this article.

Data availability

The mass spectrometry proteomics data generated in this study have been deposited in the iProX database under accession codes IPX0005800000 and subproject IPX0005800001, both associated with the ProteomeXChange PXD code: PXD056311. The data can be accessed at PXD056311, IPX0005800000 and IPX0005800001. Source data are provided with this paper.

Code availability

All code for data analysis associated with the current paper is available at https://doi.org/10.5281/zenodo.13846294[76].

References

1. Ostrom, Q. T. et al. The epidemiology of glioma in adults: a "state of the science" review. *Neuro Oncol.* **16**, 896–913 (2014).
2. Louis, D. N. et al. The 2016 World Health Organization Classification of Tumors of the Central Nervous System: a summary. *Acta Neuropathol.* **131**, 803–820 (2016).
3. Louis, D. N. et al. The 2021 WHO Classification of Tumors of the Central Nervous System: a summary. *Neuro Oncol.* **23**, 1231–1251 (2021).
4. Brennan, C. W. et al. The somatic genomic landscape of glioblastoma. *Cell* **155**, 462–477 (2013).
5. Ceccarelli, M. et al. Molecular profiling reveals biologically discrete subsets and pathways of progression in diffuse glioma. *Cell* **164**, 550–563 (2016).
6. Cancer Genome Atlas Research Network Comprehensive genomic characterization defines human glioblastoma genes and core pathways. *Nature* **455**, 1061–1068 (2008).
7. Oh, S. et al. Integrated pharmaco-proteogenomics defines two subgroups in isocitrate dehydrogenase wild-type glioblastoma with prognostic and therapeutic opportunities. *Nat. Commun.* **11**, 3288 (2020).
8. Yang, K. et al. Glioma targeted therapy: insight into future of molecular approaches. *Mol. Cancer* **21**, 39 (2022).
9. Varn, F. S. et al. Glioma progression is shaped by genetic evolution and microenvironment interactions. *Cell* **185**, 2184–2199.e16 (2022).
10. Verhaak, R. G. et al. Integrated genomic analysis identifies clinically relevant subtypes of glioblastoma characterized by abnormalities in PDGFRA, IDH1, EGFR, and NF1. *Cancer Cell* **17**, 98–110 (2010).
11. Sanson, M. et al. Isocitrate dehydrogenase 1 codon 132 mutation is an important prognostic biomarker in gliomas. *J. Clin. Oncol.* **27**, 4150–4154 (2009).
12. Hegi, M. E. et al. MGMT gene silencing and benefit from temozolomide in glioblastoma. *N. Engl. J. Med.* **352**, 997–1003 (2005).
13. Cairncross, G. et al. Phase III trial of chemoradiotherapy for anaplastic oligodendroglioma: long-term results of RTOG 9402. *J. Clin. Oncol.* **31**, 337–343 (2013).
14. Yanovich-Arad, G. et al. Proteogenomics of glioblastoma associates molecular patterns with survival. *Cell Rep.* **34**, 108787 (2021).
15. Wang, L. B. et al. Proteogenomic and metabolomic characterization of human glioblastoma. *Cancer Cell* **39**, 509–528.e20 (2021).
16. Zhang, B. et al. Proteogenomic characterization of human colon and rectal cancer. *Nature* **513**, 382–387 (2014).
17. Mertins, P. et al. Proteogenomics connects somatic mutations to signalling in breast cancer. *Nature* **534**, 55–62 (2016).
18. Zhang, H. et al. Integrated proteogenomic characterization of human high-grade serous ovarian cancer. *Cell* **166**, 755–765 (2016).
19. Dong, L. et al. Proteogenomic characterization identifies clinically relevant subgroups of intrahepatic cholangiocarcinoma. *Cancer Cell* **40**, 70–87.e15 (2022).
20. Wu, H. L. et al. Targeting nucleotide metabolism: a promising approach to enhance cancer immunotherapy. *J. Hematol. Oncol.* **15**, 45 (2022).
21. Pavlova, N. N. & Thompson, C. B. The emerging hallmarks of cancer metabolism. *Cell Metab.* **23**, 27–47 (2016).
22. Burhans, W. C. & Weinberger, M. DNA replication stress, genome instability and aging. *Nucleic Acids Res.* **35**, 7545–7556 (2007).
23. Shelton, J. et al. Metabolism, biochemical actions, and chemical synthesis of anticancer nucleosides, nucleotides, and base analogs. *Chem. Rev.* **116**, 14379–14455 (2016).
24. Rich, T. A., Shepard, R. C. & Mosley, S. T. Four decades of continuing innovation with fluorouracil: current and future approaches to fluorouracil chemoradiation therapy. *J. Clin. Oncol.* **22**, 2214–2232 (2004).
25. Mager, L. F. et al. Microbiome-derived inosine modulates response to checkpoint inhibitor immunotherapy. *Science* **369**, 1481–1489 (2020).
26. Halbrook, C. J. et al. Macrophage-released pyrimidines inhibit gemcitabine therapy in pancreatic cancer. *Cell Metab.* **29**, 1390–1399.e6 (2019).
27. Vijayan, D. et al. Targeting immunosuppressive adenosine in cancer. *Nat. Rev. Cancer* **17**, 709–724 (2017).
28. Sabbah, A. et al. Activation of innate immune antiviral responses by Nod2. *Nat. Immunol.* **10**, 1073–1080 (2009).
29. Giuliani, A. L., Sarti, A. C. & Di Virgilio, F. Extracellular nucleotides and nucleosides as signalling molecules. *Immunol. Lett.* **205**, 16–24 (2019).
30. Mullen, N. J. & Singh, P. K. Nucleotide metabolism: a pan-cancer metabolic dependency. *Nat. Rev. Cancer* **23**, 275–294 (2023).
31. Kim, K. H. et al. Integrated proteogenomic characterization of glioblastoma evolution. *Cancer Cell* **42**, 358–377.e8 (2024).
32. Guo, X. et al. Comprehensive analysis of sterol O-acyltransferase 1 as a prognostic biomarker and its association with immune infiltration in glioma. *Front. Oncol.* **12**, 896433 (2022).
33. Ferreira, W. A. S. et al. Comprehensive analysis of epigenetics regulation, prognostic and the correlation with immune infiltrates of GPX7 in adult gliomas. *Sci. Rep.* **12**, 6442 (2022).
34. Yang, W. et al. Potentiating the antitumour response of CD8(+) T cells by modulating cholesterol metabolism. *Nature* **531**, 651–655 (2016).
35. Weinberg, S. E. et al. Mitochondrial complex III is essential for suppressive function of regulatory T cells. *Nature* **565**, 495–499 (2019).
36. Field, C. S. et al. Mitochondrial integrity regulated by lipid metabolism is a cell-intrinsic checkpoint for treg suppressive function. *Cell Metab.* **31**, 422–437.e5 (2020).
37. Qie, J. et al. Integrated proteomic and transcriptomic landscape of macrophages in mouse tissues. *Nat. Commun.* **13**, 7389 (2022).
38. Waitkus, M. S., Diplas, B. H. & Yan, H. Isocitrate dehydrogenase mutations in gliomas. *Neuro Oncol.* **18**, 16–26 (2016).
39. L, M. G. et al. Oncogenic activities of IDH1/2 mutations: from epigenetics to cellular signaling. *Trends Cell Biol.* **27**, 738–752 (2017).

40. Chen, R. et al. Hominoid-specific enzyme GLUD2 promotes growth of IDH1R132H glioma. *Proc. Natl. Acad. Sci. USA* **111**, 14217–14222 (2014).

41. Zhang, I. Y. et al. RAGE ablation attenuates glioma progression and enhances tumor immune responses by suppressing galectin-3 expression. *Neuro Oncol.* **25**, 886–898 (2023).

42. Yang, Y. et al. Identification of neural progenitor cell-associated chemoradiotherapy resistance gene set (ARL4C, MSN, TNFAIP6) for prognosis of glioma. *Curr. Pharm. Des.* **28**, 2189–2202 (2022).

43. Wang, Y. et al. FABP5 enhances malignancies of lower-grade gliomas via canonical activation of NF-kappaB signaling. *J. Cell Mol. Med.* **25**, 4487–4500 (2021).

44. Han, M. Z. et al. TAGLN2 is a candidate prognostic biomarker promoting tumorigenesis in human gliomas. *J. Exp. Clin. Cancer Res.* **36**, 155 (2017).

45. Shirahata, M. et al. Novel, improved grading system(s) for IDH-mutant astrocytic gliomas. *Acta Neuropathol.* **136**, 153–166 (2018).

46. Iuchi, T. et al. Clinical significance of the 2016 WHO classification in Japanese patients with gliomas. *Brain Tumor Pathol.* **35**, 71–80 (2018).

47. Hanahan, D. & Weinberg, R. A. Hallmarks of cancer: the next generation. *Cell* **144**, 646–674 (2011).

48. Bjorkblom, B. et al. Distinct metabolic hallmarks of WHO classified adult glioma subtypes. *Neuro Oncol.* **24**, 1454–1468 (2022).

49. Lafita-Navarro, M. C. et al. Inhibition of the de novo pyrimidine biosynthesis pathway limits ribosomal RNA transcription causing nucleolar stress in glioblastoma cells. *PLoS Genet.* **16**, e1009117 (2020).

50. Wang, W. et al. Targeting pyrimidine metabolism in the era of precision cancer medicine. *Front. Oncol.* **11**, 684961 (2021).

51. Richards, L. M. et al. Gradient of developmental and injury response transcriptional states defines functional vulnerabilities underpinning glioblastoma heterogeneity. *Nat. Cancer* **2**, 157–173 (2021).

52. Bader, J. M. et al. Proteomics separates adult-type diffuse high-grade gliomas in metabolic subgroups independent of 1p/19q codeletion and across IDH mutational status. *Cell Rep. Med.* **4**, 100877 (2023).

53. Willson, J. Gliomas lean on pyrimidines. *Nat. Rev. Cancer* **22**, 606–607 (2022).

54. Shi, D. D. et al. De novo pyrimidine synthesis is a targetable vulnerability in IDH mutant glioma. *Cancer Cell* **40**, 939–956.e16 (2022).

55. Pal, S. et al. A druggable addiction to de novo pyrimidine biosynthesis in diffuse midline glioma. *Cancer Cell* **40**, 957–972.e10 (2022).

56. Kato, H. et al. DPYD, down-regulated by the potentially chemopreventive agent luteolin, interacts with STAT3 in pancreatic cancer. *Carcinogenesis* **42**, 940–950 (2021).

57. Siddiqui, A. & Ceppi, P. A non-proliferative role of pyrimidine metabolism in cancer. *Mol. Metab.* **35**, 100962 (2020).

58. Marangoni, E. et al. Capecitabine efficacy is correlated with TYMP and RB1 expression in PDX established from triple-negative breast cancers. *Clin. Cancer Res.* **24**, 2605–2615 (2018).

59. Gao, Y. et al. Chemotherapy-induced CDA expression renders resistant non-small cell lung cancer cells sensitive to 5′-deoxy-5-fluorocytidine (5′-DFCR). *J. Exp. Clin. Cancer Res.* **40**, 138 (2021).

60. Tarar, A., Alyami, E. M. & Peng, C. A. Mesenchymal stem cells anchored with thymidine phosphorylase for doxifluridine-mediated cancer therapy. *RSC Adv.* **11**, 1394–1403 (2021).

61. Li, W. & Yue, H. Thymidine phosphorylase: a potential new target for treating cardiovascular disease. *Trends Cardiovasc. Med.* **28**, 157–171 (2018).

62. Fukushima, M. et al. Structure and activity of specific inhibitors of thymidine phosphorylase to potentiate the function of antitumor 2′-deoxyribonucleosides. *Biochem. Pharmacol.* **59**, 1227–1236 (2000).

63. Liekens, S. et al. The nucleoside derivative 5′-O-trityl-inosine (KIN59) suppresses thymidine phosphorylase-triggered angiogenesis via a noncompetitive mechanism of action. *J. Biol. Chem.* **279**, 29598–29605 (2004).

64. Hamzic, S. et al. Fluoropyrimidine chemotherapy: recommendations for DPYD genotyping and therapeutic drug monitoring of the Swiss Group of Pharmacogenomics and Personalised Therapy. *Swiss Med. Wkly.* **150**, w20375 (2020).

65. Paladhi, A. et al. Targeting thymidine phosphorylase alleviates resistance to dendritic cell immunotherapy in colorectal cancer and promotes antitumor immunity. *Front. Immunol.* **13**, 988071 (2022).

66. World Medical, A. World Medical Association Declaration of Helsinki: ethical principles for medical research involving human subjects. *JAMA* **310**, 2191–2194 (2013).

67. Guo, T. et al. Rapid mass spectrometric conversion of tissue biopsy samples into permanent quantitative digital proteome maps. *Nat. Med.* **21**, 407–413 (2015).

68. Cai, X. et al. High-throughput proteomic sample preparation using pressure cycling technology. *Nat. Protoc.* **17**, 2307–2325 (2022).

69. Cai, X. et al. PulseDIA: data-independent acquisition mass spectrometry using multi-injection pulsed gas-phase fractionation. *J. Proteome Res.* **20**, 279–288 (2021).

70. Meier, F. et al. diaPASEF: parallel accumulation-serial fragmentation combined with data-independent acquisition. *Nat. Methods* **17**, 1229–1236 (2020).

71. Mertins, P. et al. Reproducible workflow for multiplexed deep-scale proteome and phosphoproteome analysis of tumor tissues by liquid chromatography-mass spectrometry. *Nat. Protoc.* **13**, 1632–1661 (2018).

72. Flavahan, W. A. et al. Brain tumor initiating cells adapt to restricted nutrition through preferential glucose uptake. *Nat. Neurosci.* **16**, 1373–1382 (2013).

73. Xie, Q. et al. Mitochondrial control by DRP1 in brain tumor initiating cells. *Nat. Neurosci.* **18**, 501–510 (2015).

74. Wang, Z. et al. The Hippo-TAZ axis mediates vascular endothelial growth factor C in glioblastoma-derived exosomes to promote angiogenesis. *Cancer Lett.* **513**, 1–13 (2021).

75. Xu, Y. P. et al. Tumor suppressor TET2 promotes cancer immunity and immunotherapy efficacy. *J. Clin. Investig.* **129**, 4316–4331 (2019).

76. Sun, R. Proteomic profiling of gliomas unveils immune and metabolism-driven subtypes with implications for anti-nucleotide metabolism therapy. *Zenodo*. https://doi.org/10.5281/zenodo.13846294 (2024).

Acknowledgements

Author contributions

Y.M., H.Y., T.G., and W.H. designed and supervised this study. J.Z., R.S. Y. Lyu and C.L. analyzed the data and organized the manuscript and figures. J.Z. and C.L. interpreted and discussed the results. Y. Liu and Z.D. performed slice staining and selected histological area for punction. T.Q., Y.Z., D.Z., Z.Q., Y.Y., and W.Z. provided the glioma samples and clinical information. R.S. performed the mass spectrometry-related experiments. Y.F., P.W. M.F., and T.G. revised the manuscript. All authors have read and approved the final manuscript.

Competing interests

T.G. is a shareholder of Westlake Omics Inc. The other authors declare no potential competing of interest.

Additional information

Jinsen Zhang[1,2,3,4,5,12], Rui Sun[6,7,8,12], Yingying Lyu[1,2,3,4,5,12], Chaxian Liu[1,2,3,4,5,12], Ying Liu[9], Yuan Feng[1,2,3,4,5], Minjie Fu[1,2,3,4,5], Peter Jih Cheng Wong [1,2,3,4,5], Zunguo Du[10], Tianming Qiu[1,2,3,4,5], Yi Zhang[1,2,3,4,5], Dongxiao Zhuang[1,2,3,4,5], Zhiyong Qin[1,2,3,4,5], Yu Yao[1,2,3,4,5], Wei Zhu [1,2,3,4,5], Tiannan Guo[6,7,8], Wei Hua [1,2,3,4,5] ✉, Hui Yang [1,2,3,4,5,11] ✉ & Ying Mao [1,2,3,4,5] ✉

[1]Department of Neurosurgery, Huashan Hospital, Fudan University, Shanghai, China. [2]National Center for Neurological Disorders, Shanghai, China. [3]Shanghai Key Laboratory of Brain Function Restoration and Neural Regeneration, Shanghai, China. [4]Neurosurgical Institute of Fudan University, Shanghai, China. [5]Shanghai Clinical Medical Center of Neurosurgery, Shanghai, China. [6]Affiliated Hangzhou First People's Hospital, State Key Laboratory of Medical Proteomics, School of Medicine, Westlake University, Hangzhou, Zhejiang, China. [7]Westlake Center for Intelligent Proteomics, Westlake Laboratory of Life Sciences and Biomedicine, Hangzhou, Zhejiang, China. [8]Research Center for Industries of the Future, School of Life Sciences, Westlake University, Hangzhou, Zhejiang, China. [9]Department of Pathology, Shanghai Medical College, Fudan University, Shanghai, China. [10]Department of Pathology, Huashan Hospital, Fudan University, Shanghai, China. [11]State Key Laboratory of Medical Neurobiology and MOE Frontiers Center for Brain Science, Institute for Translational Brain Research, Shanghai Medical College, Fudan University, Shanghai, China. [12]These authors contributed equally: Jinsen Zhang, Rui Sun, Yingying Lyu, Chaxian Liu. ✉e-mail: hs_huawei@126.com; hui_yang@fudan.edu.cn; maoying@fudan.edu.cn